Available online at www.sciencedirect.com
SCIENCE DIRECT®
International Journal of Thermal Sciences 45 (2006) 567–578
International Journal of Thermal Sciences
www.elsevier.com/locate/ijts

Numerical simulation of double-diffusive mixed convection within a rotating horizontal annulus

Abdalla M. Al-Amiri [a], Khalil M. Khanafer [b,*]

[a] *Department of Mechanical Engineering, The United Arab Emirates University, PO Box 17555, Al-Ain, United Arab Emirates*
[b] *Biomedical Engineering Department, University of Michigan, Ann Arbor, MI 48109, USA*

Received 3 November 2004; accepted 12 September 2005

Available online 25 October 2005

Abstract

A numerical investigation of double-diffusive mixed convection within a two-dimensional, horizontal annulus has been carried out. The outer cylinder was made to rotate in an anti-clockwise direction to introduce the forced convection effect. In addition, the solutal and thermal buoyancy forces are sustained by maintaining the inner cylinder at a uniform but higher concentration and temperature values, respectively. The flow is considered to operate in the laminar regime under steady state conditions. Moreover, the transport equations are solved using the Galerkin weighted residual method by incorporating a non-uniform mesh size. The heat and mass transfer rates were closely examined using several dimensionless groups in a wide domain of operating conditions. The considered domains in this investigation are as follows: $5 \leqslant Re \leqslant 150$, $0.01 \leqslant Le \leqslant 10$, $10^3 \leqslant Ra \leqslant 10^5$, $-15 \leqslant N \leqslant 15$, $0.7 \leqslant Pr \leqslant 10$, $0.5 \leqslant \sigma \leqslant 5$ and $-0.75 \leqslant \varepsilon \leqslant 0.75$. The whole flow regimes were defined according to the relative values of Reynolds number and solutal and thermal Grashof number. Furthermore, the predictions of the average Nusselt and Sherwood numbers were obtained for the operating range of the Lewis and buoyancy ratio numbers.

Keywords: Double-diffusive flow; Rotating annulus; Mixed convection; Two-dimensional; Numerical

1. Introduction

Double-diffusive convection is generally referred to the class of problems where the fluid flow is induced by the simultaneous presence of two diffusive components, namely; temperature and concentration [1]. A substantial amount of research has been reported on double-diffusive convection in confined spaces due to its vast engineering applications. For instance, the technologies involved in the chemical vapor deposition processes for the semiconductor device fabrications [2]. Also, the migration of impurities in non-isothermal material processing applications has motivated many researchers in exploring the characteristics of the associated species and energy transport processes. The effect of rotation in a double-diffusive convection has been considered in natural phenomena (e.g., atmospheric and oceanic flow) and several engineering applications. The migration of the species is known to be sensitive to the magnitude of rotational speed, which is a crucial parameter in drying technologies and crystal growth applications. Furthermore, the incorporation of rotation effects introduces Taylor vortices due to the presence of a centrifugal force, which is essential in order to control the dynamics of the system at hand. Other pertinent technologies include melting and solidification processes in a steadily rotating furnace are likely candidates for such applications. In addition, the flow and heat transfer characteristics under the simultaneous effect of temperature and concentration gradients are determined by the combined effects of inertia, flow buoyancy and centrifugal forces. These effects are generally represented by the Grashof number and the 'rotational' Reynolds number, respectively. It is a common practice to present the combined effect of both numbers in terms of Richardson number; which is the ratio of Grashof number to Reynolds number. This term indicates the importance of the buoyancy forces to the rotational ones and its impact on the flow and heat transfer within the considered system. Another important parameter is

* Corresponding author.
E-mail addresses: alamiri@uaeu.ac.ae (A.M. Al-Amiri), khanafer@umich.edu (K.M. Khanafer).

1290-0729/$ – see front matter
doi:10.1016/j.ijthermalsci.2005.09.001

Nomenclature

C'	concentration ..... $\mathrm{kg\cdot m^{-3}}$
C	dimensionless concentration, $(C' - C'_o)/(C'_i - C'_o)$
e_r, e_ϕ	unit vectors in the radial and angular directions, respectively.
e	vertical eccentricity of the inner cylinder ..... m
D	mass diffusivity ..... $\mathrm{m^2\cdot s^{-1}}$
g	gravitational acceleration ..... $\mathrm{m\cdot s^{-2}}$
Gr_S	solutal Grashof number, $g\beta_S \Delta C'(r_o - r_i)^3/\nu^2$
Gr_T	thermal Grashof number, $g\beta_T \Delta T(r_o - r_i)^3/\nu^2$
k	thermal conductivity ..... $\mathrm{W\cdot m^{-1}\cdot K^{-1}}$
Le	Lewis number, Sc/Pr
N	buoyancy ratio number, Gr_S/Gr_T
Nu	Nusselt number
p	pressure ..... $\mathrm{N\cdot m^{-2}}$
P	dimensionless pressure
Pr	Prandtl number, ν/α
r	radial coordinate
r_i, r_o	radii of the inner and outer cylinders, respectively
R_i, R_o	dimensionless radii of the inner and outer cylinders, respectively
Ra	Rayleigh number, $g\beta\Delta T(r_o - r_i)^3/\nu\alpha$
Re	Reynolds number, $r_o\omega(r_o - r_i)/\nu$
Sc	Schmidt number, ν/D
Sh	Sherwood number
t	time ..... s
T	temperature ..... K
$\mathbf{u}$	dimensionless velocity vector
$\mathbf{v}$	velocity vector ..... $\mathrm{m\cdot s^{-1}}$
u, v	dimensionless velocity components in the radial and angular directions, respectively

Greek symbols

α	thermal diffusivity ..... $\mathrm{m^2\cdot s^{-1}}$
β_S	solutal expansion coefficient ..... $\mathrm{m^3\cdot kg^{-1}}$
β_T	thermal expansion coefficient ..... $\mathrm{K^{-1}}$
ε	dimensionless vertical eccentricity of the inner cylinder, $e/(r_o - r_i)$
ϕ	angular coordinate
σ	ratio of the inner cylinder diameter to the gap width, $2r_i/(r_o - r_i)$
ν	fluid kinematic viscosity ..... $\mathrm{m^2\cdot s^{-1}}$
Ψ	dimensionless stream function
θ	dimensionless temperature, $(T - T_o)/(T_i - T_o)$
ρ	density ..... $\mathrm{kg\cdot m^{-3}}$
ω	angular velocity ..... $\mathrm{rad\cdot s^{-1}}$
Ω	dimensionless vorticity, $\omega(r_o - r_i)/U_o$
τ	dimensionless time, $\omega r_o t/(r_o - r_i)$

Subscripts

i	inner cylinder
o	outer cylinder

the buoyancy ratio number, which accounts for the strength of the concentration gradient to its thermal counterpart.

The transport processes involved in double-diffusive flows are configured based on the orientation of the externally imposed temperature and solutal gradients. Ostrach [3] has pointed out that various convection modes can emerge based on the orientations of the temperature and concentration gradients. Most of the surveyed studies in the literature were concerned primarily with the double-diffusive natural convection in rectangular cavities [4–7]. Alleborn et al. [8] and Wang and Wei [9] outlined some of the major studies in this regard. Furthermore, a lesser number of investigations were reported on the double-diffusive convection in a horizontal annulus. Ship et al. [10] conducted a numerical study for steady laminar double-diffusive natural convection within a vertically mounted closed annulus with constant temperature and mass species differences imposed across the vertical walls. Their results showed that the buoyancy ratio was the primary parameter that defined the flow structure. Later on, the same authors [11] studied the effect of thermal Rayleigh number and Lewis number on double-diffusive natural convection in a closed annulus. The results illustrated that the thermal Rayleigh number and the Lewis number were found to influence the buoyancy ratios at which flow transition and flow reversal occurred. In addition, several studies were reported on double-diffusive convection in a vertical annulus. Lee et al. [12,13] have investigated, among others, the effect of rotation in a double-diffusive convection for a stably stratified fluid within an annulus. The effect of rotation on the development and merging of the multi-layered flow structure and various field variables were presented. Furthermore, Sung et al. [14] reported on a rotating horizontal annulus configuration, where the external temperature gradient is imposed horizontally while the solutal gradient is applied in the vertical direction. They conducted a parametric study to present the qualitative features of flow patterns and isotherms.

The present study investigates the flow and heat transfer characteristics of a binary fluid within a two-dimensional horizontal annulus with cooled rotating outer cylinder. In addition, the flow is assumed to operate in the laminar regime under steady state conditions. Double-diffusive mixed convection is maintained by taking the inner cylinder as the heated wall and the source for the species concentration as well. The analyses of the pertinent field variables are presented for various essential parameters such as the Reynolds number, Lewis number, Buoyancy ratio number, Rayleigh number, Prandtl number, the annulus gap width ratio, and the eccentricity factor. These parameters will be examined over a broad range to present the basic flow patterns and isotherms in cylindrical geometries. The domains of the dimensionless parameters used in the present study were within the range of values used by many authors in the literature for mixed convection heat transfer in a two-dimensional annulus (see, for instance, Refs. [15–17]).

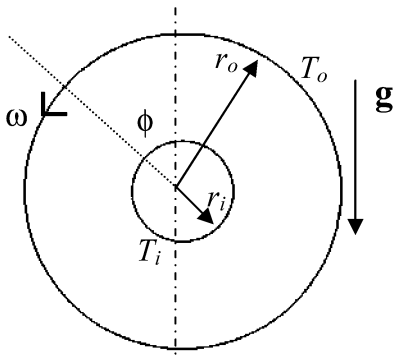

Fig. 1. Schematic of the physical model and coordinate system.

2. Mathematical model

The schematic diagram of the horizontal annulus along with the pertinent boundary conditions is shown in Fig. 1. The inner cylinder of radius r_i and the outer cylinder of radius r_o are kept at uniform and constant temperatures (T_i andT_o) and concentrations (C_i' and C_o'), respectively, with $T_i > T_o$ and $C_i' > C_o'$. The inner cylinder is fixed, while the outer cooled cylinder is kept on rotating in the counter-clockwise direction with a constant angular velocity ω. In addition, the flow in the annular region is assumed to be two-dimensional, steady and laminar. Also, all thermophysical properties of the fluid are taken to be constant except for the density variation in the buoyancy term, where the Boussinesq approximation is considered to be linearly proportional with both temperature and concentration such that:

$$\rho = \rho_o\big[1 - \beta_T(T - T_o) - \beta_s(C - C_o)\big] \tag{1}$$

where β_T and β_s are the coefficients for thermal and concentration expansions, respectively such that:

$$\beta_T = -\frac{1}{\rho_o}\left(\frac{\partial\rho}{\partial T}\right)_{P,C'} \quad \text{and} \quad \beta_s = -\frac{1}{\rho_o}\left(\frac{\partial\rho}{\partial C'}\right)_{P,T} \tag{2}$$

Dimensionless variables and dimensionless numbers are introduced as follows to cast the governing equations in dimensionless forms:

$$R_i = \frac{r_i}{r_o - r_i}, \qquad R_o = \frac{r_o}{r_o - r_i}$$
$$\mathbf{u} = \frac{\mathbf{v}}{\omega r_o}, \qquad \theta = \frac{T - T_o}{T_i - T_o}, \qquad C = \frac{C' - C_o'}{C_i' - C_o'}$$
$$P = \frac{p}{\rho_o(\omega r_o)^2} \quad \text{and} \quad \tau = \frac{\omega r_o t}{r_o - r_i} \tag{3}$$

The dimensionless forms of the governing equations, which describe the fluid motion, energy and species transports in the annulus, are given by:

$$\nabla.\mathbf{u} = 0 \tag{4}$$

$$\frac{\partial\mathbf{u}}{\partial\tau} + (\mathbf{u}.\nabla)\mathbf{u} = -\nabla P + \frac{1}{Re}\nabla^2\mathbf{u} + \frac{Gr_T}{Re^2}\big[(\theta + NC)\cos(\phi)e_r - (\theta + NC)\sin(\phi)e_\phi\big] \tag{5}$$

$$\frac{\partial\theta}{\partial\tau} + (\mathbf{u}.\nabla)\theta = \frac{\nabla^2\theta}{Pr\,Re} \tag{6}$$

$$\frac{\partial C}{\partial\tau} + (\mathbf{u}.\nabla)C = \frac{\nabla^2 C}{Sc\,Re} \tag{7}$$

where $\mathbf{u}$ is the dimensionless velocity vector, P is the dimensionless acting pressure, $Re = \omega r_o(r_o - r_i)/\nu$ is the rotational Reynolds number, $N = \beta_s\Delta C'/\beta_T\Delta T = Gr_s/Gr_T$ is the buoyancy ratio number, $Sc = \nu/D$ is the Schmidt number, $Pr = \nu/\alpha$ the Prandtl number, whereas $Gr_s = g\beta_s(C_i' - C_o')(r_o - r_i)^3/\nu^2$ and $Gr_T = g\beta_T(T_i - T_o)(r_o - r_i)^3/\nu^2$ are the solutal and thermal Grashof numbers, respectively.

For the initial conditions, the fluid temperature and concentration in the entire domain has the same temperature and concentration as the corresponding reference values at the cold wall. In addition, the no-slip condition is imposed along the solid impermeable walls. For the boundary conditions, the temperature and concentration gradients are maintained by considering higher magnitudes at the inner cylinder. The initial and boundary conditions are expressed mathematically as:

$$\begin{aligned} &u = v = \theta = C = 0 && \text{at } \tau = 0\\ &u = v = 0, \quad \theta = C = 1 && \text{at } R = R_i\\ &u = 0, \quad v = 1, \quad \theta = C = 0 && \text{at } R = R_o \end{aligned} \tag{8}$$

Upon invoking the vorticity-stream function formulation, the dimensionless velocity components in the governing equations are replaced with the dimensionless vorticity Ω and the stream function Ψ as follows:

$$\frac{\partial\Omega}{\partial\tau} = J(\Psi,\Omega) + \frac{1}{Re}\nabla^2\Omega + \frac{Gr_T}{Re^2}\left[(\theta + N)\cos(\phi)\frac{\partial\theta}{R\partial\phi} - (\theta + N)\sin(\phi)\frac{\partial\theta}{\partial R}\right] \tag{9}$$

$$\nabla^2\Psi = -\Omega \tag{10}$$

$$\frac{\partial\theta}{\partial\tau} = J(\Psi,\Omega) + \frac{1}{Pr\,Re}\nabla^2\theta \tag{11}$$

$$\frac{\partial C}{\partial\tau} = J(\Psi,\Omega) + \frac{1}{Sc\,Re}\nabla^2 C \tag{12}$$

where the dimensionless vorticity Ω, stream function Ψ, are defined as

$$\Omega = \frac{\partial(RV)}{R\partial R} - \frac{\partial(U)}{R\partial\phi}$$
$$U = \frac{\partial\Psi}{R\partial\phi} \quad \text{and} \quad V = -\frac{\partial\Psi}{\partial R} \tag{13}$$

while the Jacobian $J(f,h)$ and Laplacian ∇^2 are

$$J(f,h) = \frac{1}{R}\left(\frac{\partial f}{\partial R}\frac{\partial h}{\partial\phi} - \frac{\partial f}{\partial\phi}\frac{\partial h}{\partial R}\right) \quad \text{and}$$
$$\nabla^2 = \frac{\partial}{R\partial R}\left(R\frac{\partial}{\partial R}\right) + \frac{\partial^2}{R^2\partial\phi^2} \tag{14}$$

Therefore, the boundary conditions for vorticity-stream function formulation can be written in as follows:

$$\begin{aligned} &\Omega = -\frac{\partial^2\Psi}{\partial R^2}, \quad \frac{\partial\Psi}{\partial R} = 0 && \text{at } R = R_i\\ &\Omega = -\frac{\partial^2\Psi}{\partial R^2} + \frac{1}{R_o}, \quad \frac{\partial\Psi}{\partial R} = -1 && \text{at } R = R_o \end{aligned} \tag{15}$$

The local Nusselt number along the inner and outer cylinders are calculated as the ratio of actual heat transfer to the pure conduction heat transfer such that

$$Nu_i(\phi) = -\left(R\frac{\partial\theta/\partial R}{Nu_{\text{cond}}}\right) = \ln\frac{R_i}{R_o}\left(R\frac{\partial\theta}{\partial R}\right)_{R=R_i} \tag{16}$$

$$Nu_o(\phi) = -\left(R\frac{\partial\theta/\partial R}{Nu_{\text{cond}}}\right) = \ln\frac{R_i}{R_o}\left(R\frac{\partial\theta}{\partial R}\right)_{R=R_o} \tag{17}$$

The average Nusselt numbers at the inner and outer cylinders integrated over the respective circumferences to yield

$$\overline{Nu}_i = \frac{1}{2\pi}\int_0^{2\pi} Nu_i(\phi)\,\mathrm{d}\phi \tag{18}$$

$$\overline{Nu}_o = \frac{1}{2\pi}\int_0^{2\pi} Nu_o(\phi)\,\mathrm{d}\phi \tag{19}$$

It is worth noting that both Nusselt number expressions in Eqs. (18) and (19) will yield the same result under steady-state conditions. Similarly, the average Sherwood numbers at the inner and outer cylinders can be obtained as follows

$$\overline{Sh}_i = \frac{1}{2\pi}\int_0^{2\pi} Sh_i(\phi)\,\mathrm{d}\phi \tag{20}$$

$$\overline{Sh}_o = \frac{1}{2\pi}\int_0^{2\pi} Sh_o(\phi)\,\mathrm{d}\phi \tag{21}$$

where

$$Sh_i(\phi) = \ln\frac{R_i}{R_o}\left(R\frac{\partial C}{\partial R}\right)_{R=R_i} \quad \text{and}$$

$$Sh_o(\phi) = \ln\frac{R_i}{R_o}\left(R\frac{\partial C}{\partial R}\right)_{R=R_o} \tag{22}$$

3. Numerical method

A finite element formulation based on the Galerkin method [18,19] is employed to solve the governing equations subject to the initial and boundary conditions for the present investigation. The highly coupled and non-linear algebraic equations resulting from the discretization of the governing equations are solved using the segregated solution algorithm. The advantage of the segregation method lies in its capability to break the global system matrix into smaller submatrices and then solve them in a sequential manner, which considerably reduce the storage requirements. Furthermore, the conjugate residual scheme is used to solve the symmetric pressure-type equation systems, while the conjugate gradient squared is used for the non-symmetric advection–diffusion type equations. A fine non-uniform grid size with an exponential growth from both walls was employed to capture the rapid changes in the dependent variables. Moreover, comprehensive numerical experimentations were also performed to assure grid-independent results for all field variables. A variable grid-size system of 81×81 was employed in the radial and circumferential directions for the present study. Further increase in the number of grid points produced essentially the same results. The solution was considered to have converged to the steady state condition when the absolute value of the maximum relative change in the field variables between two consecutive iterations was less than 10^{-5}.

4. Results and discussion

The discussions presented here is pertinent to the steady state results obtained from the false transient solutions of the governing equations coupled with the set of initial and boundary conditions. The grid sensitivity analysis was performed to inspect the field variables grid-independency solutions. The results reported by Yoo [20] on mixed convection of air in concentric cylinders were used to benchmark them against the outcome of our code. The results are presented in Fig. 2 in terms of the streamline and isotherm patterns for a Rayleigh number $Ra = 10^4$ with an annulus gap of $\sigma = 2$. As shown in Fig. 2, the comparisons for $Re = 100$ and 200 are in excellent agreements, which provide sufficient confidence in the numerical algorithm.

Different scenarios were explored to exemplify the effect of a number of key dimensionless groups on the steady state flow, temperature and concentration patterns as well as the average Nusselt and Sherwood numbers. These groups include the rotational Reynolds number, Lewis number, buoyancy ratio number, Rayleigh number, Prandtl number, the implications of the annulus gap width, and the eccentricity factor. Most of the cases were performed with $Pr = 0.7$ and $\sigma = 2$ unless it is specified otherwise. In all the executed cases, the bounds of recirculation intensity were recorded for the presented streamline results to highlight the flow activity levels.

The effect of the rotational Reynolds number, which is introduced by the rotation of the outer cylinder in a counterclockwise fashion, is shown in Fig. 3 for $Ra = 10^3$, $N = 1$ and $\sigma = 2$. In order to highlight the effect of Re alone, the Lewis number was set to unity, i.e., $Pr = Sc$. The Reynolds number was varied in the range from 5 to 150 to cover a broad range of possible scenarios. For a low Reynolds number of $Re = 5$ (free convection dominant regime), the flow is primarily induced by the buoyancy force sustained by the application of the temperature gradient. This results in the formation of the famous pair of 'crescent-shaped' symmetric cells, which closely resemble the configuration of natural convection for a low Rayleigh number in an annulus. However, the symmetry here appears to be slightly distorted by the rotational effect. Giving that the rotation is in counter clockwise direction; the forced convection aids the flow in the left region of the annulus as compared to opposing it in the right side region. In addition, the viscous forces maintained by the rotation of the outer cylinder elongate the cells on the left side and drag them downwards. Subsequently, the cells on the right are pushed upwards. The isotherms echo such observations as noted by the formation of slightly titled thermal plumes in the direction of rotation. The heat convection strength weakens near the outer cylinder in the

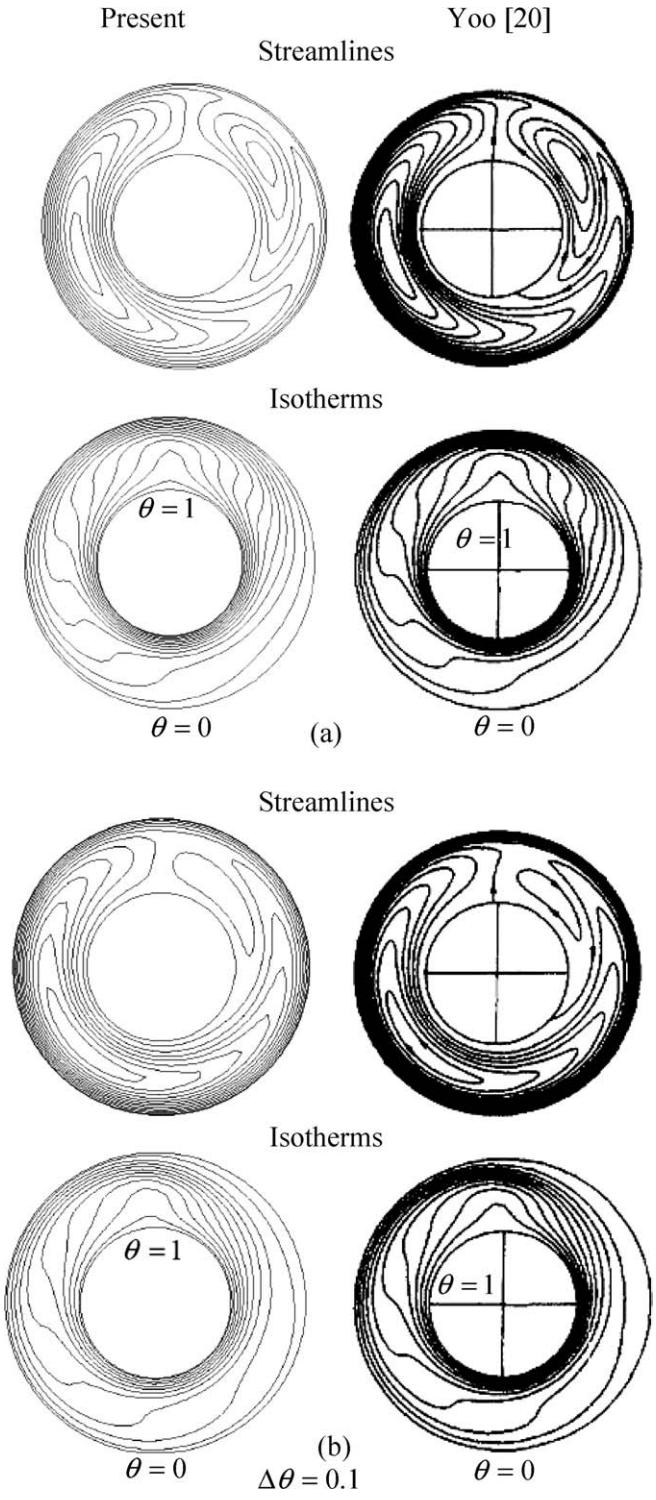

Fig. 2. Comparisons of the streamlines and isotherms between the present work and Yoo [20] for $Ra = 10^4$, $Pr = 0.7$, $\sigma = 2$ and (a) $Re = 100$ and (b) $Re = 200$.

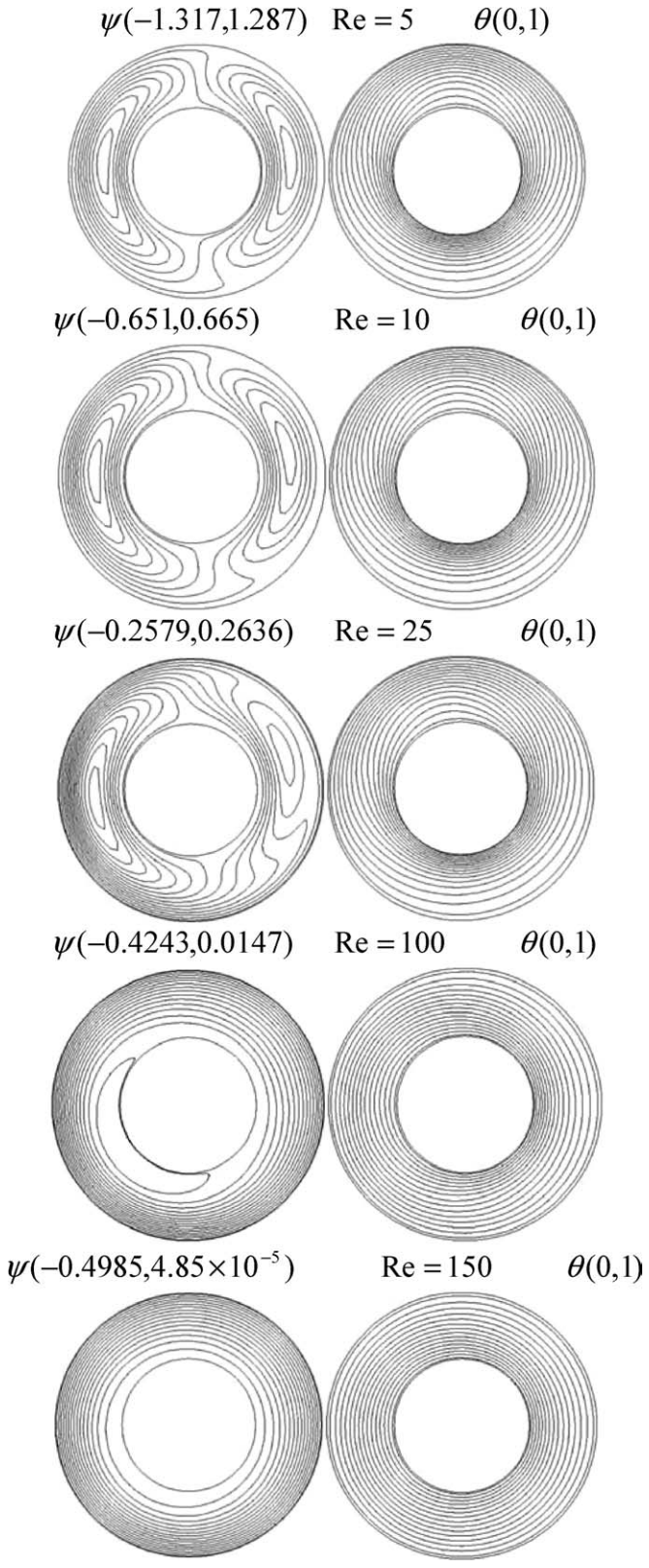

Fig. 3. Effect of rotational Reynolds number on the streamlines and isotherms for $Ra = 10^3$, $Le = N = 1$, $Pr = 0.7$ and $\sigma = 2$.

region of $\pi/2 < \phi < 3\pi/2$ owing to the decrease in flow activities.

Once the rotational Reynolds number is raised to 10 and then to 25 (mixed convection regime), the above set of observations becomes more pronounced. Upon further increase in the rotational speed, the viscous drag induced by rotation overwhelms the convective strength. As a result, the basic flow patterns depreciate in value as denoted by corresponding drop in the magnitude of the streamline levels. The increased drag offered by the large cell in the left side region creates a zone

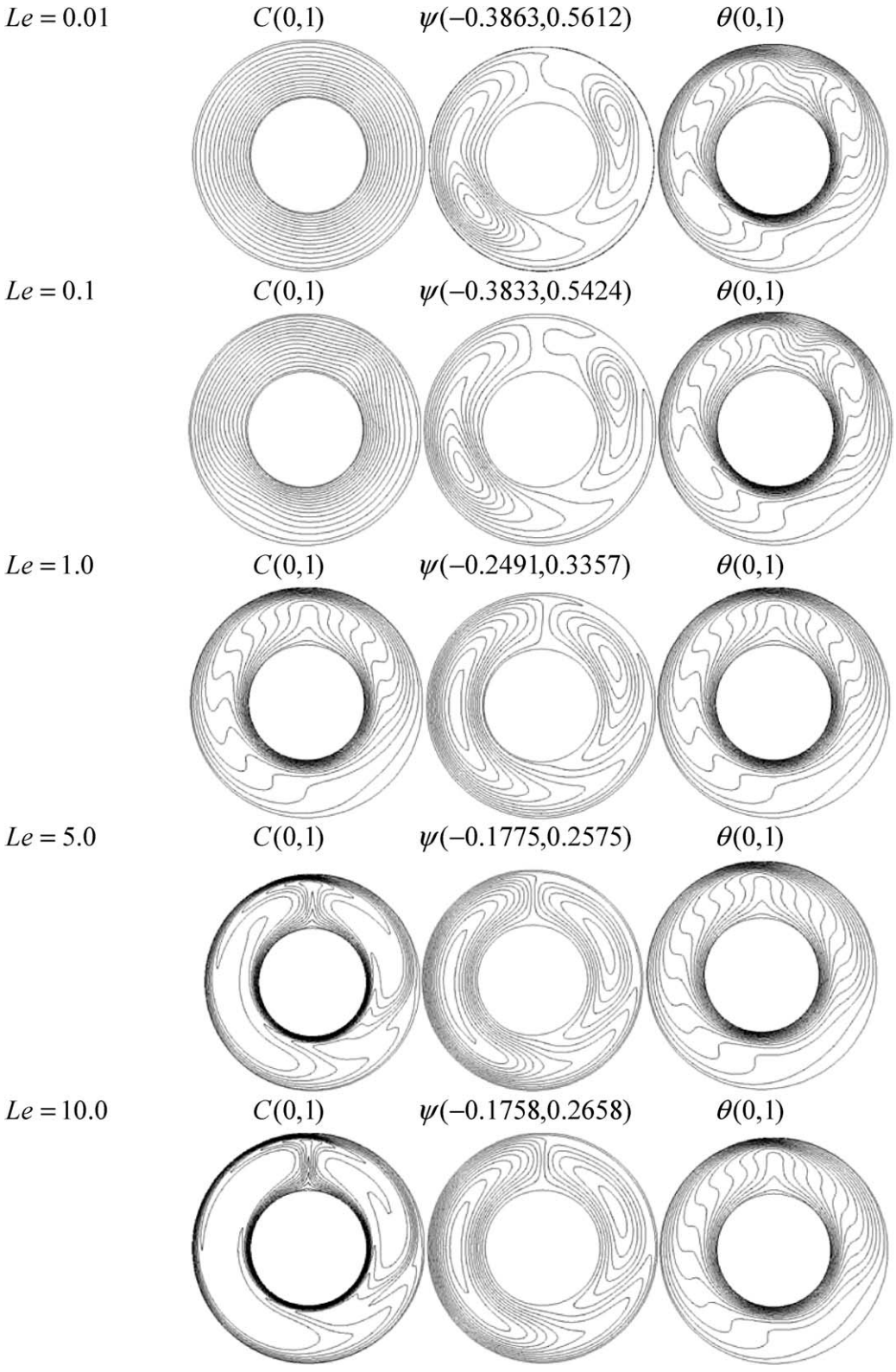

Fig. 4. Effect of Lewis number on the isoconcentrations, streamlines, and isotherms for $Ra = 10^4$, $Re = 100$, $N = 1$, $Pr = 0.7$ and $\sigma = 2$.

of a relatively low-speed flow, which brings about the domination of the conduction regime. Moreover, the results show that the separating streamline of $\Psi = 0$ has moved to the lower left region at $Re = 100$ (dominant forced convection). This further suppresses the eddy presence, which appears to fully vanish at $Re = 150$. What is more, the streamlines become similar to the classical Couette flow patterns giving their formation in circular rings around the inner cylinder. Thus, an increase in Reynolds number reduces the two-eddies flow pattern to a single-eddy one. It is note worthy that the maximum recirculation has in-

creased at $Re = 150$ (dominant forced convection), which is attributed to the domination of the mechanical rotation on the flow movement. The isotherms at high rotational speed, as a result, carry diffusion characteristics as noted by the presence of thermal stratification in the radial direction. It is worth noting that the mass diffusion characteristics will follow the same patterns reported for the thermal characteristics as the rotational speed is varied since Le was set to unity.

The dependence of heat and species transport on the Lewis number is displayed in Fig. 4. The Lewis number provides a measure of thermal diffusivity of a fluid to its mass diffusivity. Thus, a large value of Lewis number reflects a relatively low mass diffusivity value. The Lewis number in the ongoing investigation was varied in the range from 0.01 to 10. In addition, the gap width σ, Re and Ra were fixed at 2, 100 and 10^4, respectively. At $Le = 0.01$, the mass diffusion rate appears to be stratified in the radial direction. In addition, a slight increase in the mass transfer rate is depicted at $Le = 0.1$. The isoconcentration and isotherms carry out the same contour patterns since they have the same diffusion characteristics at $Le = 1$ as explained earlier. 'Concentration' plumes are observed to emerge above the inner cylinder, which signal an increase in the mass transfer rate. Also, thinner solutal boundary layers are observed to cluster under the inner cylinder, which indicates a substantial increase in the mass transfer rate. This is beneficial when a drying process is involved. This observation is further manifested as Le value was elevated to 10 (dominant mass transfer regime). The basic flow patterns show depreciation in its intensity with the increase in Le value. This is marked by the drag of the cells on the left region downward and onto the right region. Furthermore, the results also point out that the effect of Le on the isotherms seems to be insignificant for $Le \geqslant 1$ as displayed in Fig. 4. For $Le < 1$, however, the thermal plumes tend to ease a bit with the increase in Le value. This is likely attributed to the fact that the combined buoyancy effects are very much dominated by the rotation of the outer cylinder.

The effect of Lewis number on the average values of Nusselt and Sherwood numbers is illustrated in Fig. 5. The increase in the prediction of Sherwood number is vivid as Le is increased (dominant mass transfer regime). On the contrary, the Nusselt number predictions show a slight dip and then assume an asymptotic value with the increase in Le. Unlike the mass transfer enhancement, the transport of energy is not improved with the increase in Le value. Again, the predictions of the Nusselt and Sherwood numbers are coincided at $Le = 1$ giving the similarity in their diffusion characteristics.

The effect of the buoyancy ratio number, which is defined as the ratio of mass buoyancy to the thermal buoyancy forces, is explored next. To demonstrate the implications of the negative and positive buoyancy ratio numbers, the isopleths of Ψ and θ are plotted in Fig. 6(a) and (b), respectively for $Ra = 10^4$, $Re = 100$ and a gap width of $\sigma = 2$. Once more, the Lewis number was set at unity to explore the diffusion characteristics upon varying N. A negative value of N indicates that the volumetric expansion coefficient with mass fraction (β_s) holds a negative value for the prescribed temperature range. At $N = -15$ (dominant mass transfer regime), the separating streamline of $\Psi = 0$

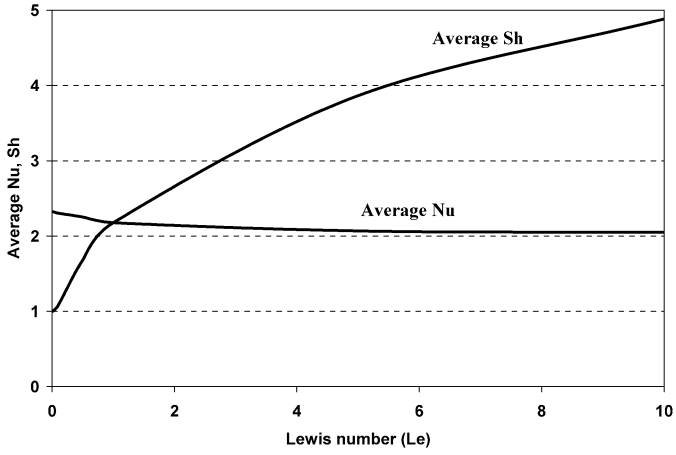

Fig. 5. Effect of Lewis number on the average Nusselt and Sherwood numbers for $Ra = 10^4$, $Re = 100$, $N = 1$, $Pr = 0.7$ and $\sigma = 2$.

in Fig. 6(a) moves to the right to encompass the large cell. Furthermore, the cells in the right region are dragged upwards and onto the left region, which brings about a drop in flow activities. The bi-thermal plumes for the negative N value have moved below the inner cylinder. Apparently, employing a negative N value causes a reversal in the basic flow patterns and isotherms. The streamlines and isotherms are both showing reverse behaviors along the horizontal centerline of the annulus as compared to the case of positive N value, which are displayed in Fig. 6(b). The flow strength further depreciates with the increase in the negative N value as the cells in the right region continue to grow in size. When the buoyancy ratio number is set to -1 (i.e., heat and mass diffusions are opposing each other), all eddies are found to disappear causing the domination of the Couette-flow patterns as discussed earlier. The thermal plumes have diffused as noted by the formation of concentric circles of isotherms. Apparently, the forced convection has overwhelmed the diffusion behaviors in the annulus. Furthermore, low streamline values are registered near the inner cylinder, which bring about the stratification of the isotherms. Upon further increase in N values, the two eddies are found to form again at $N = 0$ in Fig. 6(b) but with the separating streamline moving to the left instead. In this case, the solutal diffusion rate is no longer coupled with the velocity and temperature fields since $\beta_s = 0$, and, hence, the problem reduces to a pure mixed thermal convection. The increase in the cell size to the left is attributed to the fact that the forced flow near the outer cylinder is aiding the buoyancy-induced flow in the region of $0 < \phi < \pi$. It is interesting also to note that the higher diffusion rates have moved downward as illustrated by the isotherm patterns. Fig. 6(b) demonstrates the results generated for positive N values. Higher flow activities and diffusion rates are attained with the increase in N. In addition, the cells in the right region grow in size, which is attributed to the reduction in the magnitude of the viscous drag in the left region as higher solutal Grashof number is imposed. Relatively speaking, the flow is much weaker in the lower region near the outer cylinder owing to the influence of the viscous drag. The effect on the isotherms is also obvious with the increase in the thermal plumes above

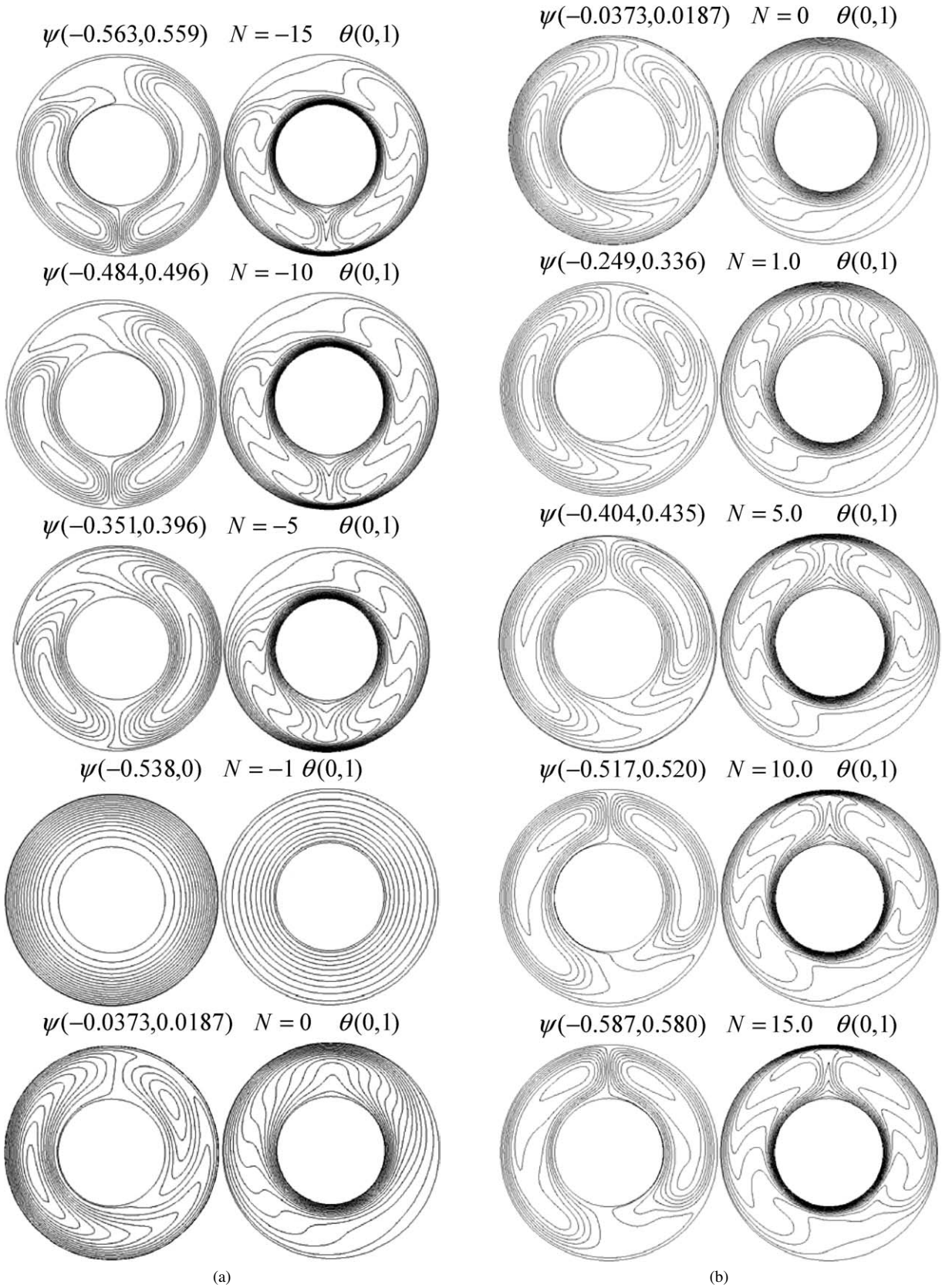

Fig. 6. (a) Effect of the negative buoyancy ratio number on the streamlines and isotherms using $Ra = 10^4$, $Re = 100$, $Le = 1$, $Pr = 0.7$ and $\sigma = 2$. (b) Effect of the positive buoyancy ratio number on the streamlines and isotherms using $Ra = 10^4$, $Re = 100$, $Le = 1$, $Pr = 0.7$ and $\sigma = 2$.

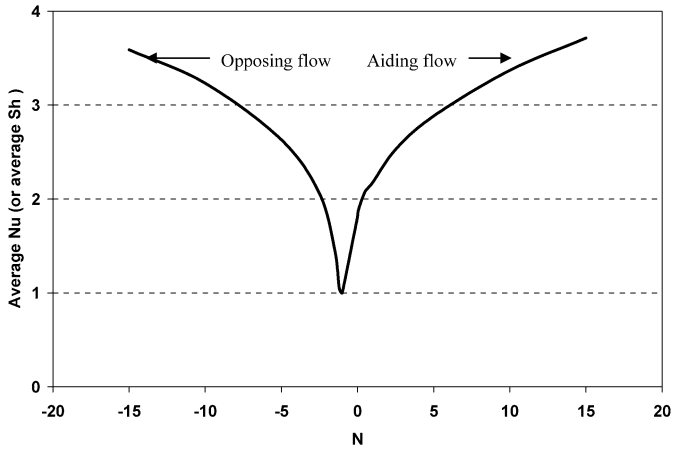

Fig. 7. Effect of buoyancy ratio number on the average Nusselt number (or Sherwood number) using $Ra = 10^4$, $Re = 100$, $Le = N = 1$, $Pr = 0.7$ and $\sigma = 2$.

the inner cylinder while the bottom region of the annulus show low transport activities.

Next, the average Nusselt number predictions over the circumference of the inner cylinder are presented for the above-mentioned dimensionless variables as shown in Fig. 7. The average Nusselt number predictions for the considered range of buoyancy ratio numbers are found to converge at $N = -1$, which represents the domination of the heat conduction regime. The results show higher Nusselt number predictions for the positive N value as compared to that for the negative N value. As can seen in Fig. 7, the Nusselt number predictions are lower in the opposing flow region than for the corresponding N value in the aiding flow range due to the combined effect of the buoyancy forces. Moreover, higher Nusselt number predictions are achieved with higher absolute values of N as, in this case, the solutal buoyancy forces contribute to the overall diffusion rate (dominant mass transfer regime).

The effect of Rayleigh number on the streamlines and isotherms is presented in Fig. 8 for $Le = N = 1$, $Re = 100$ with a gap width $\sigma = 2$. The Rayleigh number provides a measure for the significance of the buoyancy force. At $Ra = 10^3$ (forced convection dominant regime), a single cell appears in the region of $0 < \phi < \pi$. At this stage, the flow is largely overwhelmed by the rotational effect, which brings about thermal stratification of the isotherms. Once Ra is elevated to 5×10^3, an additional cell emerges and thermal plumes are observed above of the inner cylinder. Apparently, the boost in Ra value increases the contributions offered by the buoyancy forces, which intensifies flow activities and, thus, results in higher heat transfer rates. This can be depicted from the streamline Ψ values registered for each Ra, which confirms such observation. It is also observed that thinner thermal boundary layers tend to besiege much of the inner cylinder as Ra is increased, which signals the change in the mode of heat transfer from conduction to convection. This is likely attributed to the suppression in the viscous forces offered by the cells in the left region. Clearly, the cells in the left region pull away from the right side with elevated Ra values.

The effect of the Prandtl number is shown in Fig. 9 for $Le = N = 1$, $Ra = 10^4$, $Re = 100$ with a gap width $\sigma = 2$. Higher values of Prandtl numbers indicate an increase in viscous diffusion as compared to its thermal counterpart. This causes an increase in the viscous drag and, consequently, suppresses the cells formation as Pr is increased. Moreover, the streamlines

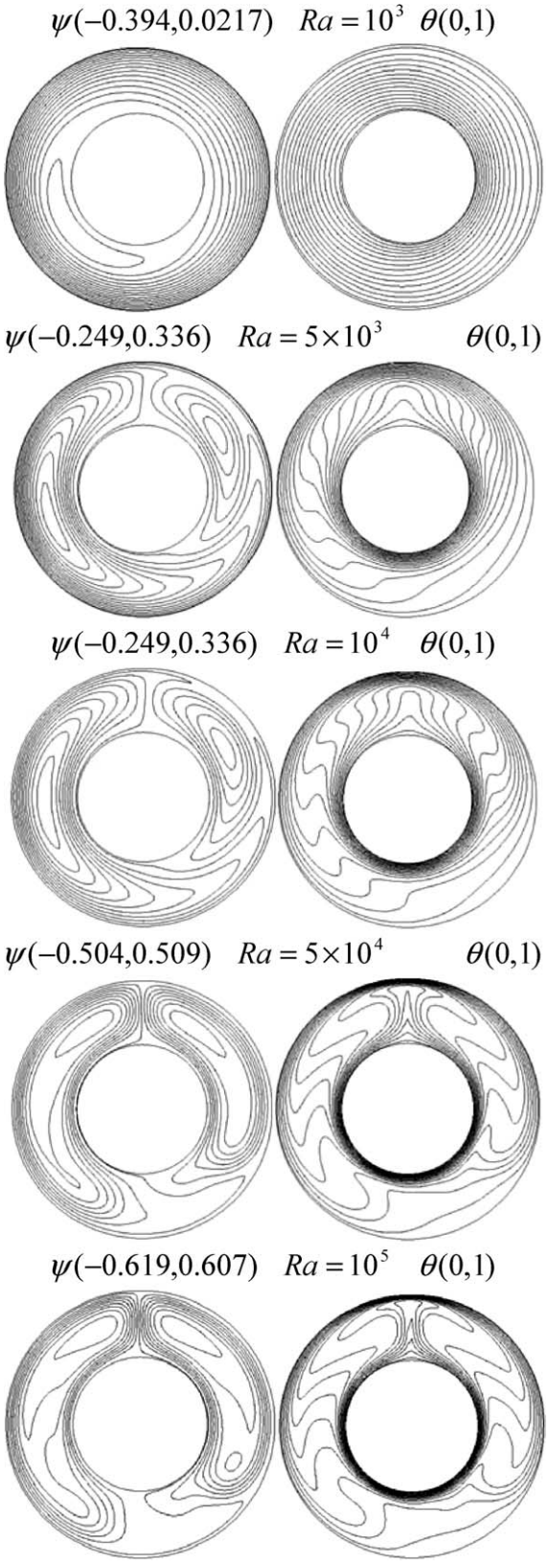

Fig. 8. Effect of Rayleigh number on the streamlines and isotherms for $Re = 100$, $Pr = 0.7$, $Le = N = 1$ and $\sigma = 2$.

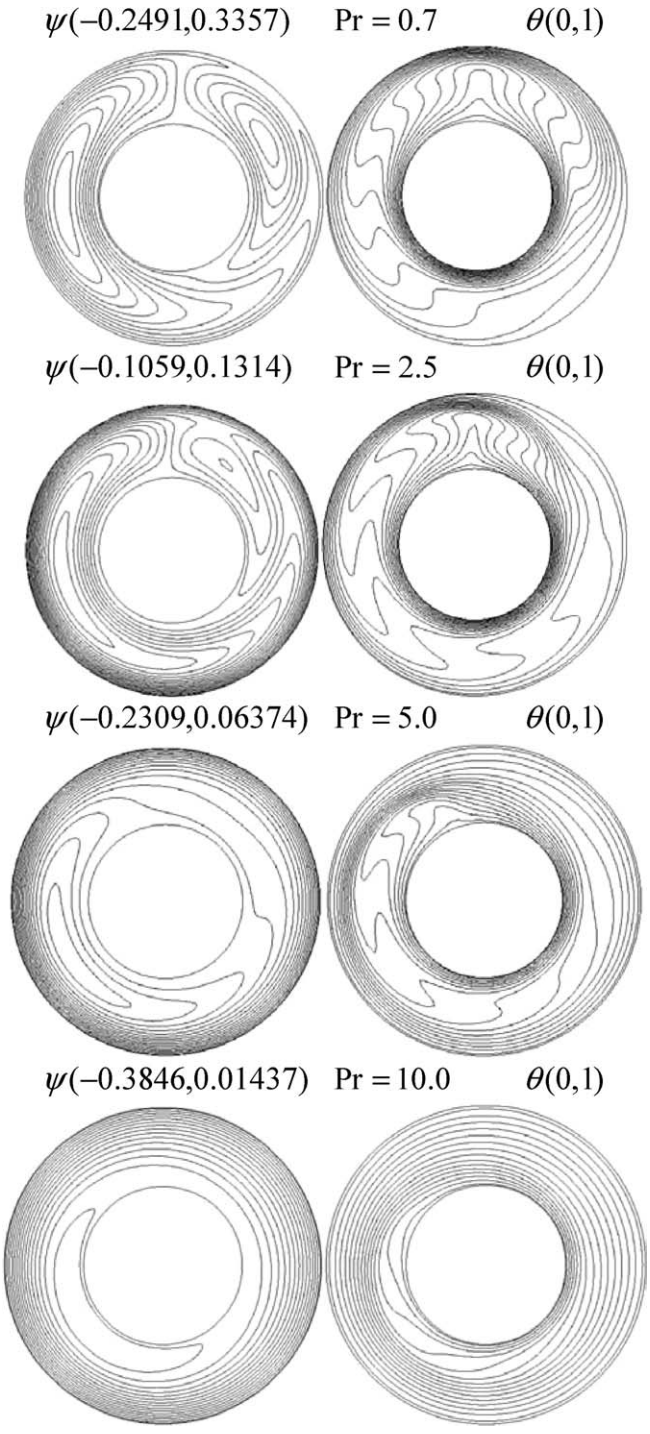

Fig. 9. Effect of Prandtl number on the streamlines and isotherms for $Ra = 10^4$, $Re = 100$, $Le = N = 1$ and $\sigma = 2$.

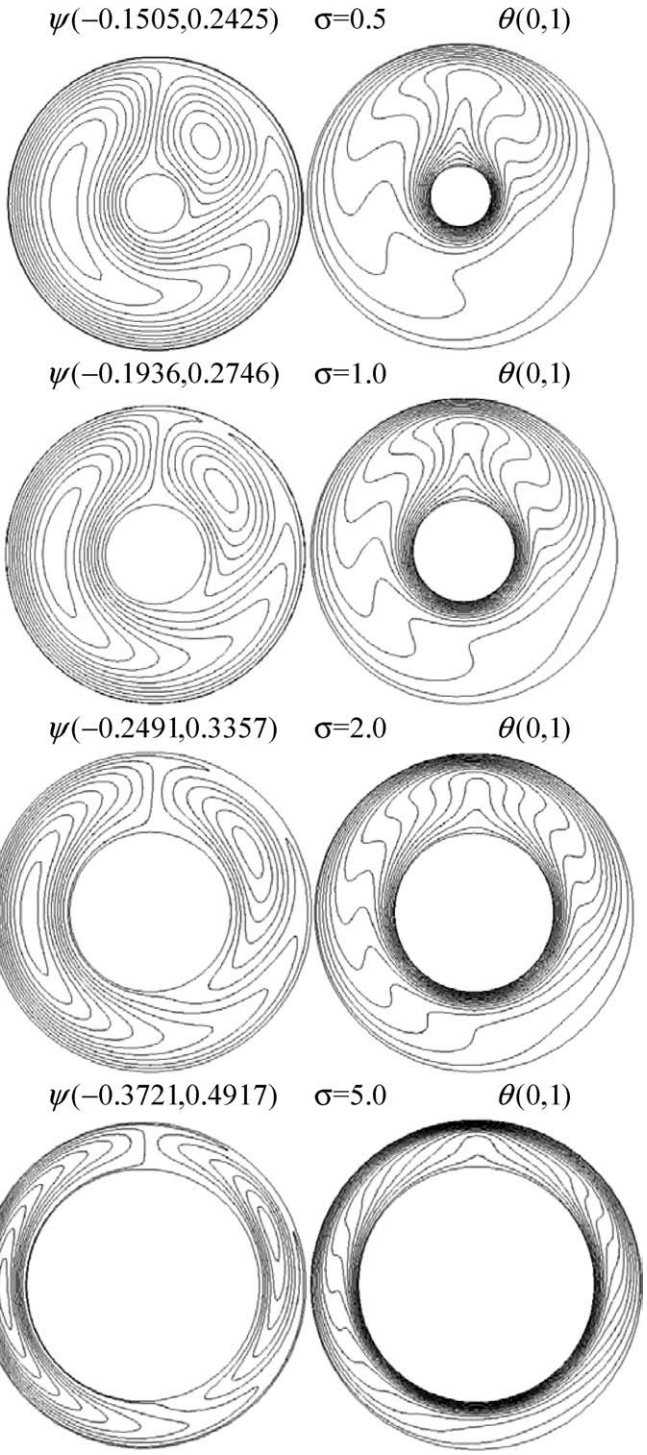

Fig. 10. Gap width effect on the streamlines and isotherms for $Ra = 10^4$, $Re = 100$, $Le = N = 1$ and $Pr = 0.7$.

and isotherms become evenly distributed with the increase in Pr value. The thermal plumes above the inner cylinder are tilted in the same direction of rotation upon increasing Pr value. This particular observation was also pointed out by Lee [21] for a laminar mixed thermal convection in an annulus.

In all the above cases, the annulus gap width σ was fixed at 2. Hence, it is important to explore the effect of the dimensionless gap width σ as well, which is varied here between 0.5 (wide gap) and 5.0 (narrow gap) as seen in Fig. 10. When the case of $\sigma = 0.5$ is considered, the gap provides an ample region for the fluid to be carried away in the annulus. The flow and thermal characteristics tend to be more convective. Moreover, the same flow and temperature patterns persist in the annulus once the gap width has increased. However, the patterns become very much confined for $\sigma = 5$, which results in the conduction regime to be more pronounced. The conduction regime is expected to dominate the transport processes for gap width

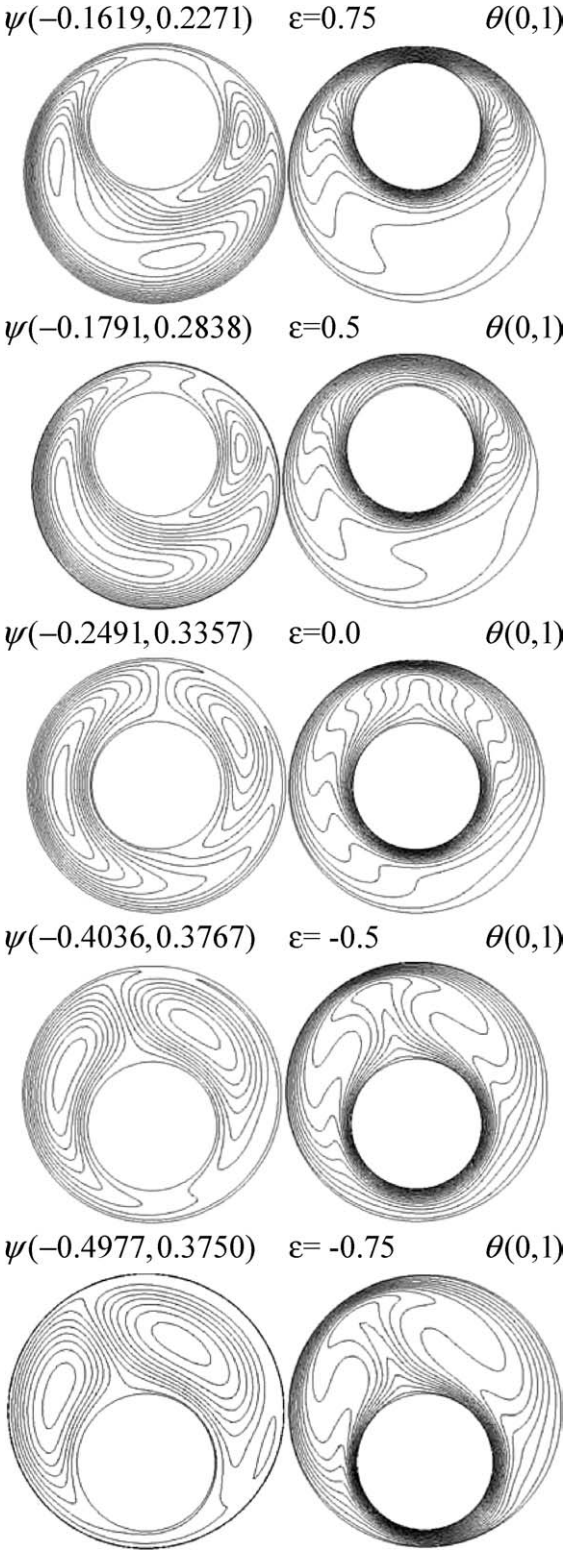

Fig. 11. Effect of eccentricity on the streamlines and isotherms for $Ra = 10^4$, $Re = 100$, $Le = N = 1$, $Pr = 0.7$ and $\sigma = 2$.

of $\sigma \geqslant 5$. The current numerical study is concluded by investigating the effect of vertical eccentricity on the rate of transport processes in the annulus as illustrated in Fig. 11. For $\varepsilon = 0.75$, the viscous drag contains much of the lower region of the annulus causing poor transport rate in the region of $0 < \phi < \pi$. When the eccentricity is reduced to 0.5, the flow activities are enhanced as denoted by the increase in the Ψ value. Thermal plumes are observed when ε is set to zero, i.e., concentric cylinder case. The eccentricity literally confines the flow cell in the direction of eccentricity, whereas more flow is allowed to 'pass' in the open area, which augments the heat transfer due to the thermal convection mechanism. The viscous drag is contained in the left region when the inner cylinder is displaced downwards. This allows the cells in the right region to penetrate to the left region to the rotational effect. As a result, flow activities intensify and the thermal plumes above the inner cylinder are enhanced and become titled in the direction of rotation.

5. Summary and conclusions

The current investigation is concerned with the numerical simulation of double diffusive flow in a two-dimensional horizontally mounted annulus with the outer cylinder rotating at a prescribed constant speed in the anti-clockwise direction. The solutal and thermal gradients were maintained by subjecting the inner cylinder to a higher magnitude than the outer one. In addition, the flow was considered laminar and under steady state conditions. The Galerkin finite element method was used to solve the set of the governing equations and the pertinent initial and boundary conditions while using a variable grid system. The investigation was carried out for a broad spectrum of relevant dimensionless groups to explore their effects on the overall flow patterns and transport rates. The employed domains of these dimensionless groups were as follows: $5 \leqslant Re \leqslant 150$, $0.01 \leqslant Le \leqslant 10$, $10^3 \leqslant Ra \leqslant 10^5$, $-15 \leqslant N \leqslant 15$, $0.7 \leqslant Pr \leqslant 10$, $0.5 \leqslant \sigma \leqslant 5$ and $-0.75 \leqslant \varepsilon \leqslant 0.75$.

The results show that high rotational Reynolds numbers tend to diffuse the thermal convection currents, which brings about the formation of the concentric-shaped isotherms. Furthermore, high Le values significantly improve the mass transfer rate, whereas it has insignificant impact on the heat transfer rate. Also, the increase in the absolute value of the buoyancy ratio number N was found to enhance the estimated Nusselt number and the Sherwood number as well. Next, the incorporation of high Prandtl number was found to stratify the isotherms, which resembles the characteristics of diffusion mode for the energy and solutal transport processes. Afterward, the effect of the annulus gap width was examined, which was observed to enhance the convective mode of the transport process upon increasing the gap width. Finally, the convective mode of heat transfer was augmented upon employing a negative eccentricity value, i.e., moving the inner cylinder downwards. The results of the present work may play an important role on enhancing the performance of many engineering applications such as drying technology and crystal growth based on a wide range of pertinent parameters studied in this work.

References

[1] J.S. Turner, Double diffusive phenomena, Annu. Rev. Fluid Mech. 6 (1974) 37–56.
[2] S. Ostrach, Fluid mechanics in crystal growth—The 1982 Freeman Scholar Lecture, J. Fluids Engrg. 105 (1983) 5–20.

[3] S. Ostrach, Natural convection with combined driving forces, Physico Chem. Hydrodyn. 1 (1980) 233–247.
[4] J. Lee, M.T. Hyun, G.W. Kim, Natural convection in confined fluids with horizontal temperature and concentration gradients, Int. J. Heat Mass Transfer 31 (1988) 1969–1977.
[5] K. Kamakura, H. Ozoe, Double-diffusive natural convection in a rectangle with horizontal temperature and concentration gradient resulting in cooperating buoyancy forces near the vertical walls, J. Materials Process. Manufacturing Sci. 5 (3) (1997) 83–196.
[6] L.W. Wang, A.T. Chai, N. Rashidnia, Ground-based experiments on thermal and thermosolutal convection in an inclined low-aspect-ratio enclosure, AIAA (1990) 90-0413.
[7] S.R. Corriell, M.R. Cordes, W.J. Baettinger, Convective and interfacial instabilities during unidirectional solidification of a binary alloy, J. Crystal Growth 49 (1980) 13–28.
[8] N. Alleborn, H. Raszillier, F. Durst, Lid-driven cavity with heat and mass transport, Int. J. Heat Mass Transfer 42 (1999) 833–853.
[9] L.W. Wang, C.Y. Wei, Natural convection heat and mass transfer in a vertical annular enclosure, in: Proc. Symposium on Transfer Phenomena and Applications, 1992, pp. 401–406.
[10] P.W. Ship, M. Shoukri, M.B. Carver, Double-diffusive natural convection in a closed annulus, Numer. Heat Transfer: Part A 24 (1993) 339–356.
[11] P.W. Ship, M. Shoukri, M.B. Carver, Effect of thermal Rayleigh and Lewis numbers on double-diffusive natural convection in a closed annulus, Numer. Heat Transfer: Part A 24 (1993) 451–465.
[12] J. Lee, S.H. Kang, Y.S. Son, Experimental study of double-diffusive convection in a rotating annulus with lateral heating, Int. J. Heat Mass Transfer 42 (1999) 821–832.
[13] J. Lee, S.H. Kang, Y.S. Son, Numerical study of multi-layered flow regime in double-diffusive convection in a rotating annulus with lateral heating, Numer. Heat Transfer: Part A 38 (2000) 467–489.
[14] H.J. Sung, W.K. Cho, J.M. Hyun, Double-diffusive convection in a rotating annulus with horizontal temperature and vertical solutal gradients, Int. J. Heat Mass Transfer 36 (1993) 3773–3782.
[15] T. Fusegi, B. Farouk, K.S. Ball, Mixed-convection flows within a horizontal concentric annulus with a heated rotating inner cylinder, Numer. Heat Transfer 9 (1986) 591–604.
[16] T.S. Lee, Numerical Experiments with laminar fluid convection between concentric and eccentric heated rotating cylinder, Numer. Heat Transfer 7 (1984) 77–87.
[17] M. Prud'Home, L. Robillard, Natural convection in an annular fluid layer rotating at weak angular velocity, Transport Phenomena Heat Mass Transfer (1992) 134–145.
[18] C. Taylor, P. Hood, A numerical solution of the Navier–Stokes equations using finite-element technique, Comput. Fluids 1 (1973) 73–89.
[19] P.M. Gresho, R.L. Lee, R.L. Sani, On the time-dependent solution of the incompressible Navier–Stokes equations in two and three dimensions, in: Recent Adv. Numer. Methods Fluids, Pineridge, Swansea, UK, 1980.
[20] J. Yoo, Mixed convection of air between two horizontal concentric cylinders with a cooler rotating outer cylinder, Int. J. Heat Mass Transfer 41 (1997) 293–302.
[21] T.S. Lee, Laminar fluid convection between concentric and eccentric heated horizontal rotating cylinders for low-Prandtl number fluids, Int. J. Numer. Methods Fluids 14 (1992) 1037–1062.